Engineering Structures 298 (2024) 117089

Contents lists available at ScienceDirect

Engineering Structures

journal homepage: www.elsevier.com/locate/engstruct

A new steel – UHPFRC composite beam with in-built composite dowels as connectors: Concept and design principles

Yaobei He [a,c], Xiujiang Shen [a,b,*], Guang Chen [c], Xudong Shao [a]

[a] College of Civil Engineering, Hunan University, Changsha, China
[b] Sustainable Materials, VITO, Boeretang 200, 2400 Mol, Belgium
[c] Hunan Provincial Communications Planning, Survey & Design Institute Co., Ltd., Changsha, Hunan 410200, China

ARTICLE INFO

Keywords:
Composite beam
UHPFRC
Rolled section
Composite dowel
In-built connector
Flexural response
Shear response
Fracture behavior
Design principle
Digital Image Correlation (DIC)

ABSTRACT

Aiming at the full and proper exploitation of both steel and Ultra High Performance cementitious Fiber Reinforced Composites (UHPFRC) materials, this paper proposes a new steel-UHPFRC composite beam structure. The unique use of ① UHPFRC in both tension and compression and ② a half rolled section with continuous in-built steel dowels in combination with UHPFRC dowels (forming composite dowels as shear connectors) is highlighted. An experimental study consisting of two composite beams is then conducted to investigate the flexural and shear responses. In particular, the failure mode, cracking pattern, and monitoring of critical crack kinematics are discussed using digital image correlation (DIC) technology. Subsequently, the design principles for both flexural and shear resistance are introduced based on the failure mechanism: ① the determination of flexural resistance is based on the sectional analysis considering the tensile properties of UHPFRC, and ② the determination of shear resistance is based on a specific approach to the lever arm of internal forces and horizontal shear resistance of the composite dowel, considering the tensile contribution of UHPFRC. According to the experimental results, the effective interlocking between UHPFRC and the steel dowel allows efficient interaction between steel and UHPFRC components, benefiting from its higher shear resistance and ductility compared with traditional welded head studs. Both the flexural and shear response of the composite beam can be characterized into five distinguished domains, in which the quasi-elastic domain is introduced especially due to its large contribution to the resistance and high structural stiffness. Finally, the design principles are validated by the tested values.

1. Introduction

The concept of sustainability is nowadays respected significantly in modern civil engineering projects relating to construction and rehabilitation of infrastructures, where minor environmental impact and low economic costs are required [1–5]. In such scenario, the advance in structural material and innovative design of structural element are the keys to fulfill this concept.

Over the past two decades, Ultra-High Performance Fiber Reinforced Concrete (UHPFRC) is well acknowledged as an advanced cementitious material with unique combination of extremely low permeability, high strength and ductility [6,7]. A notable feature of UHPFRC under tension is the significant deformation capacity including hardening strain up to 5 ‰, where only multiple microcracks (matrix discontinuities in the bulk matrix) are observed before reaching the tensile strength. Afterward, the pronounced softening behavior is characterized by the formation of one fictitious crack with major fracture energy dissipation [8,9]. Furthermore, UHPFRC shows a fatigue endurance limit up to multimillion cycles under both tension and compression [10–15]. These characteristics make UHPFRC fundamentally different from traditional concrete, and suitable ideally as structural material to improve the effectiveness, durability and sustainability of new or existing structures [16,17].

Moreover, through appropriate combination of both materials, the steel-UHPFRC composite structure has the great potentiality to develop more elegant and slender filigree element compared with conventional steel–concrete composite member in bridge engineering [18]. This aligns nicely in the field of Accelerated Bridge Construction (ABC), and can additionally lead to multiple advantages (e.g., improvement of serviceability and extension of service life). At present, the steel-UHPFRC composite structure is a relatively new solution in bridge

* Corresponding author at: Sustainable Materials, VITO, Boeretang 200, 2400 Mol, Belgium.
E-mail address: xiujiang.shen@vito.be (X. Shen).

https://doi.org/10.1016/j.engstruct.2023.117089
Received 15 August 2023; Received in revised form 9 October 2023; Accepted 22 October 2023

engineering, and deserves further investigations. The main challenges of the concept include: (1) proper geometry and arrangement of UHPFRC and steel components to fully utilize both materials; (2) robust shear connectors to ensure efficient interaction between two components.

Several studies have been conducted to implement this concept in the form of steel-UHPFRC composite beam structure over last decade, a detailed review is available in the literature [18]. As shown in Fig. 1(b), by simply replacing concrete slab with UHPFRC slab, the self-weight of steel-UHPFRC composite beam can be reduced by more than 40 %, while the cracking and ultimate resistance are increased by more than 300 % and 20 %, compared with traditional solution (Fig. 1(a)) [19–22]. More recently, Shao et al. [23,24] proposed a roll section – UHPFRC composite beam structure (Fig. 1(c)), where part of UHPFRC web contributed to flexural tension under positive moment. This resulted in lower steel consumption (reduced by 27 %) and construction cost (reduced by 24 %) over the traditional solution. On the other hand, the existing steel-UHPFRC composite beam structures can still be further optimized, given that: (1) UHPFRC is generally arranged in compression zone leading to waste of tensile properties of UHPFRC; (2) the upper flange of I-shaped steel component might be superfluous due to its position located at around the neutral axis of composite beam. Furthermore, the light-weight steel-UHPFRC composite structure maybe susceptible to fatigue issues due to the potential welding weakness of steel component and widely used welded headed studs as connectors, especially with ever-increasing traffic load and volume.

Furthermore, steel dowels in combination with concrete dowels (forming composite dowels), as a new form of continuous shear connector, have been developed and applied successfully in steel-–concrete composite structures [25–29]. As shown in Fig. 2, there are mainly four types of steel dowels depending on shape. They are now limited to two basic geometries, namely puzzle (PZ) and modified clothoid (MCL) shapes (Fig. 2(c) and (d)), due to their symmetric geometry and better fatigue resistance compared with the rest. They can be produced and built on the steel component directly through single cutting without welding on the upper flange of steel component. Also, they enable fast installation of reinforcing bars, and exhibit higher resistance and ductility compared with headed studs. In addition, it was reported that the composite dowels can still maintain sufficient levels of ductility as the concrete strength increases, especially in the case of UHPFRC [30,31].

Accordingly, combining the concept of steel-UHPFRC composite structure with composite dowel, this paper firstly proposes a steel-UHPFRC composite beam with in-built composite dowels as connector, aiming at utilizing fully both materials. An experimental study consisting of two composite beams is conducted to investigate the flexural and shear responses. Especially, the failure mode, cracking pattern, and monitoring of critical crack kinematics, are discussed additionally by using the digital image correlation (DIC) technology. Finally, the design principles, including the flexural resistance based on the sectional design model and the shear resistance through the internal lever arm, are introduced and validated based on the experiment results.

2. Conceptual design of a new steel-UHPFRC composite beam structure

As illustrated in Fig. 3, the new steel-UHPFRC composite beam structure consists of an inverted T-shaped steel component with in-built continuous steel dowels and a T-shaped UHPFRC component with steel reinforcement. The steel component is produced as a half from I-shaped rolled section by single cutting (automatic oxygen cutting, laser cutting, etc.), and the cutting line forms the continuous steel dowels directly. Hence, two identical steel components with in-built dowels can be generated from one rolled section through single cutting. And the steel dowels are inserted into the web of T-shaped UHPFRC component, forming steel-UHPFRC composite dowel, to create connection between two components.

In such context, compared with conventional steel–concrete composite beam under positive moment (the most usual support condition for small and medium span bridges), the new structure is expected to exploit the best properties of both materials (Fig. 4):

(1) The single-flange steel component, whose relative ineffective steel part near the neutral axis is removed, is arranged in the high tension zone to resist large part of the flexural tensile stress.
(2) Upper part (top flange mainly) of UHPFRC component is in compression zone to resist the entire compressive stress, and the lower part of UHPFRC web contributes to part of tensile resistance.
(3) The hot rolled section with low residual stress during manufacturing is used and divided into two identical steel components with in-built continuous steel dowels by single cutting. Thus, no welding procedure is required, leading to fast fabrication and assembly, as well as reducing risk of fatigue failure.

3. Experimental investigation

3.1. Tested elements and preparation

To validate the proposed concept of the new composite structure as described above, an experimental programme has been conducted to investigate its response in flexure and shear, respectively. It consists of two composite beams with different lengths, as illustrated in Fig. 5. The longer beam (B1) with length of 4.0 m is designed for flexural failure using 4-point bending test (4PBT) with a length of 450 mm in constant moment zone, the vertical stirrups are intensively arranged (spacing of 100 mm, $\Phi = 8$ mm) in the shear-bending zone to avoid undesired shear failure during testing. It should be mentioned that B1 is subjected to positive moments during testing, considering that this is the most usual support condition for small and medium span bridges. The shorter beam (B2) with length of 3.0 m is designed for shear failure using 3-point

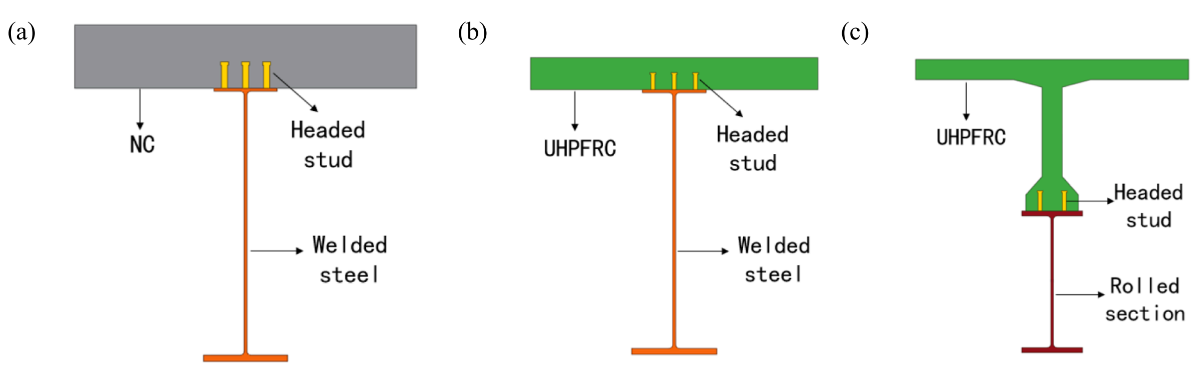

Fig. 1. Cross-section of: (a) traditional steel–concrete beam; and (b,c) steel-UHPFRC composite beams.

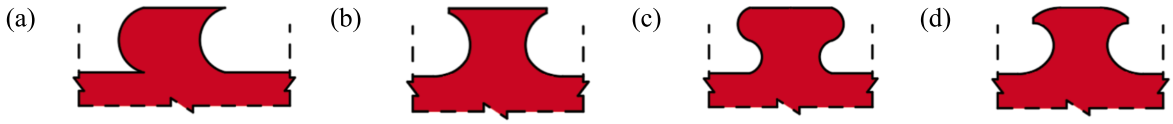

Fig. 2. Shapes of different steel dowels: (a) fin (SA), (b) clothoid (CL), (c) puzzle (PZ), and (d) modified clothoid (MCL).

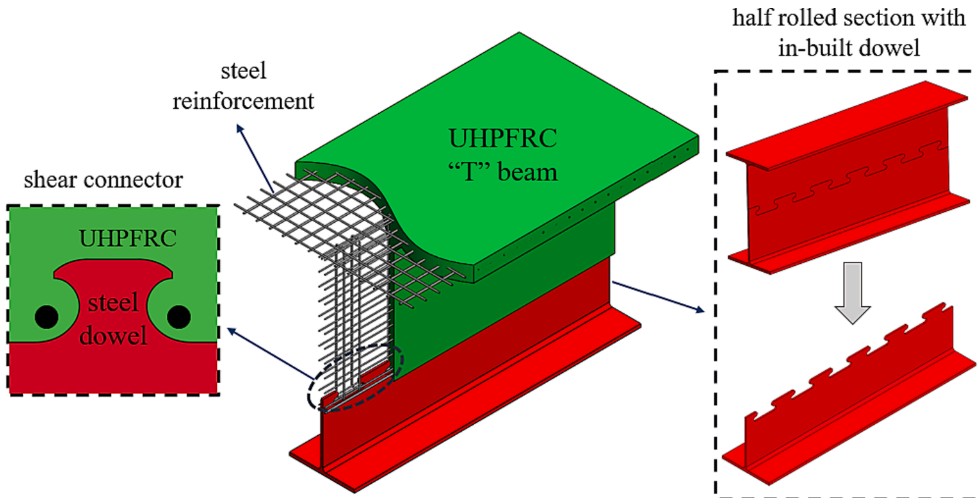

Fig. 3. Schematic illustration of proposed steel-UHPFRC composite beam structure.

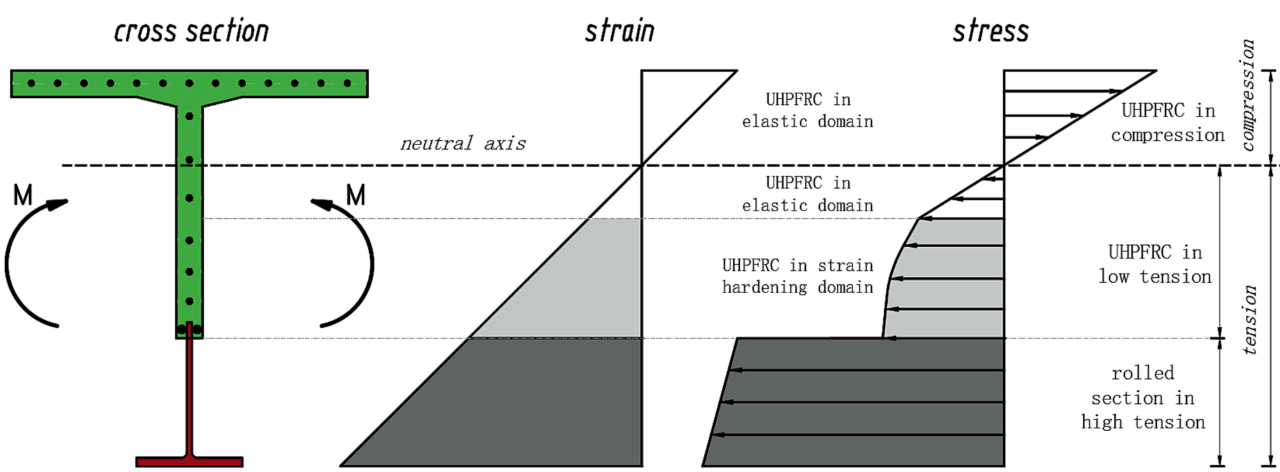

Fig. 4. Distribution of strain and stress in cross-section.

bending test (3PBT), with the critical shear span length a = 1300 mm, corresponding to a shear slenderness ratio of 2. The cross-sections of two beams are shown in Fig. 5 (c) and (d), which are almost same except the steel flange on bottom. In the case of B1, the steel flange is cut intentionally to 100 mm to ensure the flexural failure, while keeping 200 mm for B2.

The steel dowels (MCL-shaped with multiple curves) are designed followed the Germany's National Technical Approval [32], as shown in Fig. 5 (e). The height of single steel dowel is 40 mm, and the spacing is 100 mm. It should be pointed out that the stirrups are arranged to pass through the recesses between dowels to improve the interaction between UHPFRC and steel dowels, thus avoiding the premature splitting failure of UHPFRC, as reported by S. Heinemeyer [33].

The rolled section was cut following a single line in the middle of the web to form two identical steel components (Fig. 5 (f)). The formwork for UHPFRC component was then built directly on the steel component. During casting, the fresh UHPFRC mixture was poured from one end and flowed freely to the other end until the whole formwork was filled up. The casting surface was then covered by plastic sheet and left in the lab-environmental condition for 48 h. Afterward, the formwork was removed, and the elements were stored curing room (≥90℃, R ≥ 95 %) for another 48 h. Finally, the elements were kept in the lab until testing.

3.2. Material and properties

The UHPFRC used in this study is an industrial premix containing 2.0 % by volume of straight steel fibers with length of 13 mm and diameter of 0.2 mm. At 28 days, the UHPFRC has an average modulus of 50GPa and compressive strength of 140 MPa, measured on cube with dimension of 100 × 100 × 100 mm.

The tensile behavior of UHPFRC was obtained using direct tensile test (DTT), as shown in Fig. 6. The DTT results are presented in Fig. 7 in terms of stress vs. strain curves, and the corresponding tensile parameters for each specimen are summarized in Table 1. In general, all

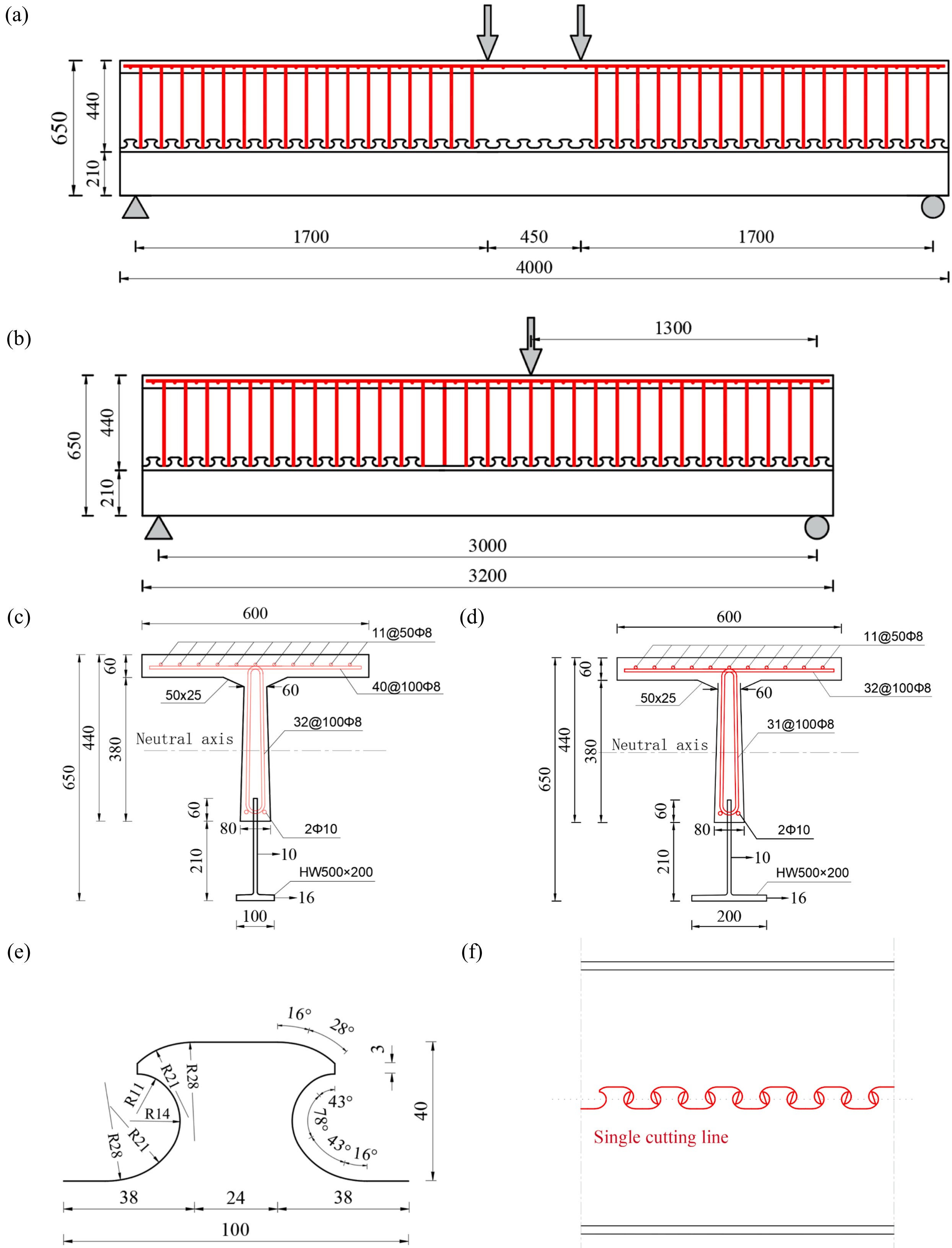

Fig. 5. Tested elements: (a) B1 for 4PBT test; (b) B2 for 3PBT; (c) cross-section of longer beam; (d) cross-section of shorter beam; (e) geometry of steel dowel; (f) single cutting line in rolled section.

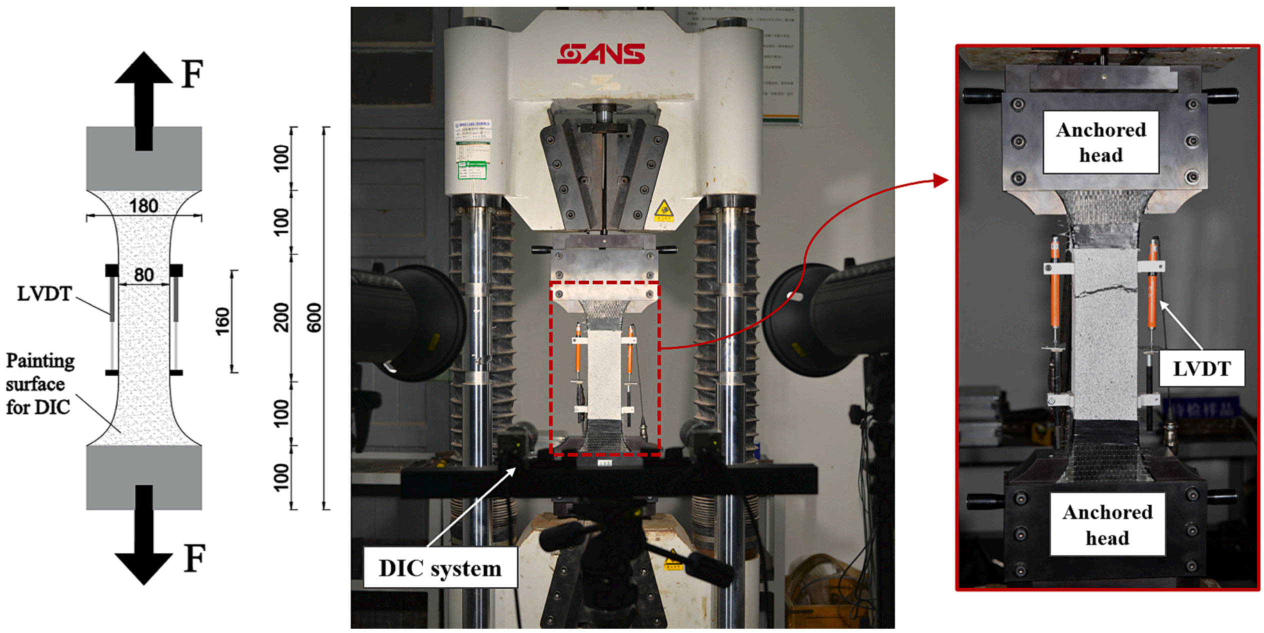

Fig. 6. Setup for direct tensile test (DTT).

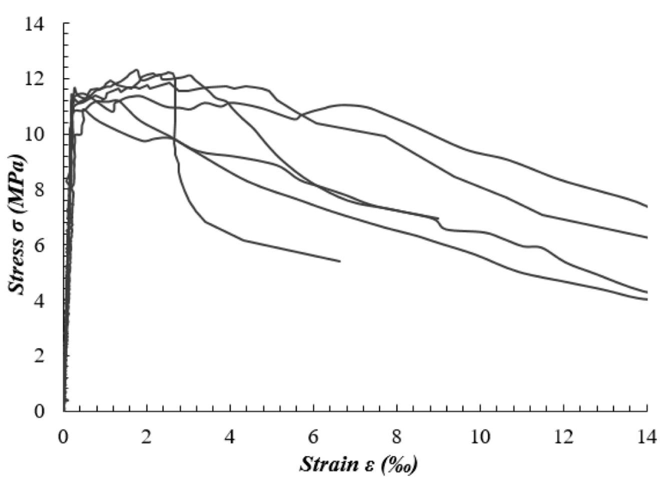

Fig. 7. Stress – strain response of 6 specimens under DTT.

specimens exhibit strain-hardening behavior with comparable values of elastic limit and ultimate strength, although the ultimate strain varies, in particular for specimens T2%-3 and T2%-5. The average response is chosen as representative properties of present UHPFRC mix for following analysis.

The H-shaped rolled section with type of HW500 × 200 and ribbed steel bars were used in the beams. The corresponding tensile properties from 3 samples for each material are shown in Table 2.

3.3. Test setup and procedure

The test configuration for 4PBT and 3PBT are shown in Fig. 8. The DIC system was used to observe the full-field strain evolution during the whole testing process: two digital cameras (5328 × 3040 Pixel) were placed on the side of the element at a distance of 600 mm and an angle of 25 degrees to the horizontal. The DIC region for 4PBT test was set in the constant moment zone (450 mm × 380 mm), while in the dominant shear crack zone (950 mm × 380 mm) for 3PBT. The targeted surface was painted with matte white paint, followed by spraying a black speckle pattern with size around 0.8 mm. In this case, the DIC measurement accuracy can reach about 5με. In addition, several Linear Variable Differential Transformers (LVDTs) were installed to measure the deflection (at the middle of the beam for 4PBT and at the loading section for 3PBT) and deformation at the supports, respectively. All deflection/deformation measurements are performed with respect to the strong floor. Furthermore, a pair of strain gauges was installed on the top and bottom of the beam at the critical section, to measure the compressive strain of UHPFRC flange top and tensile strain of steel flange bottom, respectively.

During testing, the displacement-controlled monotonic loading was applied by a 2000kN hydraulic jack, at a rate equal to 0.5 mm/min. The recordings of the two cameras of the DIC system were synchronized via wired computer control with a frequency of 0.2 Hz, while the recording by the LVDTs and strain gauge was 5 Hz.

4. Experimental results and discussion

4.1. Flexural behavior

4.1.1. Failure mode and force vs. Deflection response

The B1 under 4PBT shows typical flexural failure mode with one dominant crack surrounded by several fictitious cracks (visible by naked eyes), as illustrated in Fig. 9, where the black lines refer to the cracks. Large opening is observed at the critical part of the dominant crack, where all fibers are pull out and the two longitudinal steel bars at the lower part of the UHPFRC web are ruptured. And the UHPFRC flange is crushed at the position of the top end of dominant crack.

Significant ductility is observed, as shown by the force–deflection (F-δ) curve in Fig. 10, in which the deflection was measured in the middle of the span excluding the deformation at the supports based on the measurement from LVDTs. Here, the ductility is defined quantitatively by a coefficient as introduced in [34]. The deflection is as large as 93.93 mm when the peak force is reached, and the beam element after peak force keeps high structural stiffness comparable with the initial value, as recognized by the scant modulus of the F-δ curve in the unloading phase. It should be noted that, the beam element was unloaded at point E due to the limited measured range of LVDT (up to 100 mm), resulting in very short softening domain (DE).

In addition, the force vs. strain relationship at the critical points of the middle section is presented in Fig. 11. It can be noted that the bottom

Table 1
Tensile properties of UHPFRC based on DTT results.

N^O	E_U [GPa]	f_{Ute} [MPa]	f_{Utu} [MPa]	f_{Utu}/f_{Ute}	ε_{Ute} [‰]	ε_{Utu} [‰]	n[1]	S_r[2] [mm]	Microcracks pattern[3]
T2%-1	45.78	10.98	11.86	1.08	0.23	4.77	18	7.83	
T2%-2	52.27	10.90	12.24	1.12	0.21	2.53	20	7.04	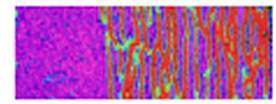
T2%-3	51.23	9.98	10.90	1.09	0.29	1.88	5	28.00	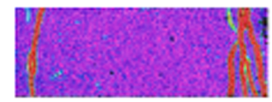
T2%-4	42.48	11.34	11.43	1.01	0.27	4.05	18	7.33	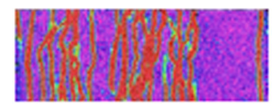
T2%-5	55.64	10.86	11.22	1.03	0.29	1.30	6	22.50	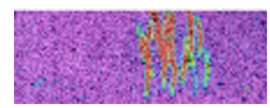
T2%-6	58.28	11.15	12.28	1.10	0.22	3.03	21	6.67	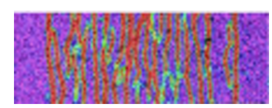
Average	50.95	10.87	11.66	1.07	0.25	2.93	15	13.23	–
Std. dev.	5.93	0.47	0.56	0.04	0.04	1.31	7	9.48	–
$\hat{c}_v$	0.12	0.04	0.05	0.04	0.14	0.45	0.49	0.72	–

[1] n is the number of microcracks on the UHPFRC surface at ultimate strength;
[2] S_r is the average spacing of microcracks on the UHPFRC surface at ultimate strength;
[3] Microcrack pattern is obtained from DIC analysis.

Table 2
Tensile properties of steel material (mean value).

Material	Grade	Dimension *[mm]*	E_s *[GPa]*	f_{sy} *[MPa]*	ε_{sy} *[×10^{-6}]*	f_{su} *[MPa]*
Rolled section	Q355	10[a]	208	381	1832	523
		16[b]	207	375	1811	512
Ribbed steel bar	HRB400	Φ10	205	437	2132	565

[a] thickness of web of rolled section (HW500 × 200);
[b] thickness of flange of rolled section (HW500 × 200).

surface of the steel flange started to yield at the force of 717kN, only 56 % of the peak force. This implies that most of the steel component entered into yielding domain at the peak force. Moreover, by assuming the linear strain distribution along the cross-section, the position of neutral axis of the composite beam (the distance from the bottom, H_n) against the imposed force is shown in Fig. 12.

4.1.2. Fracture behavior based on DIC analysis

Based on DIC analysis using VIC-3D software, the fracture behavior of the UHPFRC web at the constant moment zone under the whole testing process was captured, as illustrated in Fig. 13. Several representative DIC strain contours are selected, where the blue and red lines represent the microcracks or fictitious cracks. It should be noted that the initiation and propagation of microcracks are invisible to naked eyes and can not be measured using traditional sensors, but are detected visually on DIC strain contours. On this basis, the F-δ curve can be characterized into 5 different domains, as marked with letters A-E in Fig. 10, namely the elastic domain (OA), quasi-elastic domain (AB), hardening domain (BC), yielding domain (CD) and softening domain (DE). Here, point A (elastic limit) is determined when the first microcrack appeared, point B (quasi-elastic limit) stands for the status when no new microcracks were generated, while point C refers to the start of strain concentration on one or several microcracks. Accordingly, the flexural parameters (force, deflection, strain on bottom and position of neutral axis) at each characteristic points are summarized in Table 3.

Furthermore, using the virtual extensometers in DIC analysis tool, the maximum opening of every single microcrack and fictitious crack was recorded over the entire testing duration. The virtual extensometers, with measurement length of about 12 mm, were set separately to be perpendicular to the propagation path and located at the critical part of each target. The force vs. maximum opening (F-w_{max}) response is shown in Fig. 14, where a large amount of microcracks ($w_{max} < 0.1$ *mm*) and several fictitious cracks are identified. It can be noted that most of the microcracks start to close partially after peak force, and the corresponding residual openings are less than 0.05 mm at the end of testing. The corresponding values of maximum opening are also given in Table 3.

In the following, the flexural response of the composite beam is described according to the five distinguished domains based on DIC

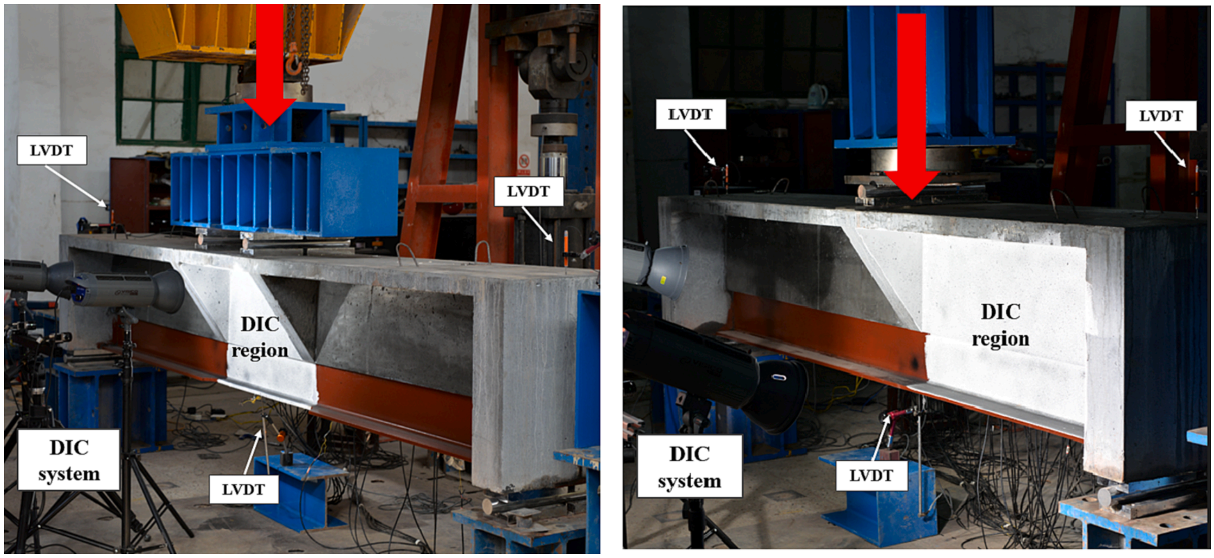

Fig. 8. Test setup and instrumentation for (a) B1; (b) B2.

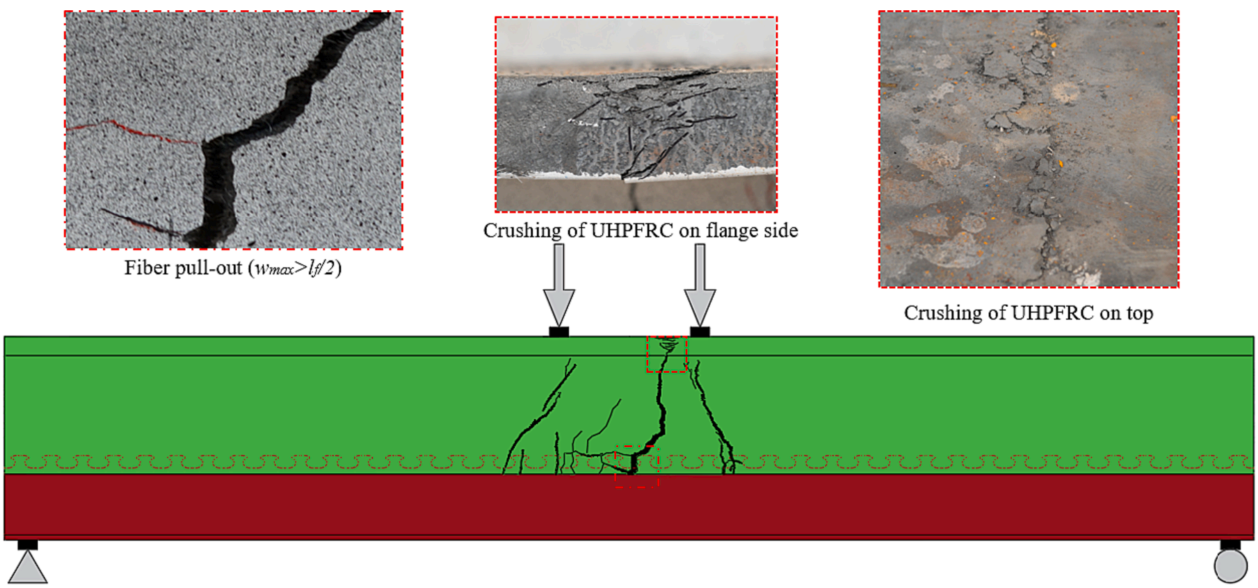

Fig. 9. Failure mode of B1 after testing.

analysis (Fig. 13 and Fig. 14) and traditional measurement results (Fig. 10, Fig. 11 and Fig. 12):

(1) Elastic domain (OA):

Both UHPFRC and steel were in elastic phase, resulting in a linear F-δ curve up to elastic limit (point A), whose force corresponded to 15 % of peak force (F_A≈0.15·F_D) and the position of neutral axis kept constant ($H_{n\text{-}A}$ = 436 mm). At this point, several microcracks initiated randomly from the lower part of the UHPFRC web in the constant moment zone as observed from the DIC strain contour. It should be noted that this point can also be determined when an irreversible decrease of 5 % of the moving scant modulus of F-δ curve was observed firstly, similar method was applied in [9,35].

(2) Quasi-elastic domain (AB).

The steel component was still in elastic phase, while part of UHPFRC in tension entered into hardening phase with multiple microcracks (w_{max} = 0.032 mm). As imposed force increased, new microcracks were generated on the UHPFRC web surface and distributed uniformly with spacing less than 20 mm at quasi-elastic limit (point B, F_B≈0.57·F_D), while the position of neutral axis moved upward moderately. It is shown that the F-δ curve almost kept linear and around 42 % of the resistance was developed in this domain.

(3) Hardening domain (BC).

As indicated in Fig. 11, the steel component started to yield, and most of the UHPFRC part in tension were in hardening phase (w_{max} = 0.058 mm). In this domain, the existing microcracks propagated upward with slow increase of opening. There were almost no new microcracks generated and the position of neutral axis increased slightly.

(4) Yielding domain (CD).

At point C (F_C≈0.67·F_D), the strain concentration appeared on several microcracks. As the force increased, these microcracks entered into softening phase and one of them became the dominant crack, while the rest kept in hardening phase with little propagation. Simultaneously, more part of steel component yielded and the position of neutral axis moved upward quickly. When the force reached 1229kN (≈0.98·F_D) and the maximum crack opening w_{max} = 5.56 mm, the first longitudinal steel rebar ruptured. Afterward, the central deflection δ and w_{max} increased

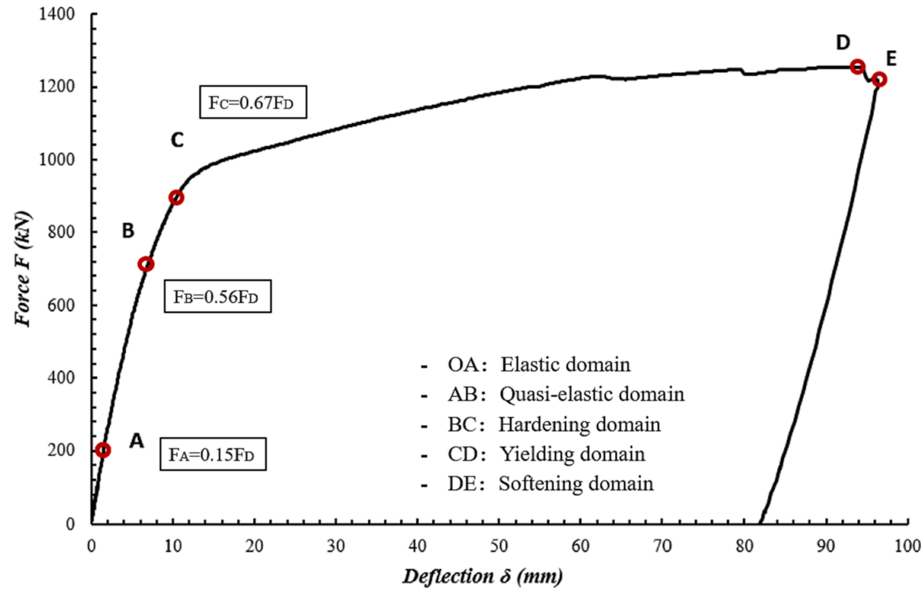

Fig. 10. Force vs. deflection (F-δ) relationship from B1.

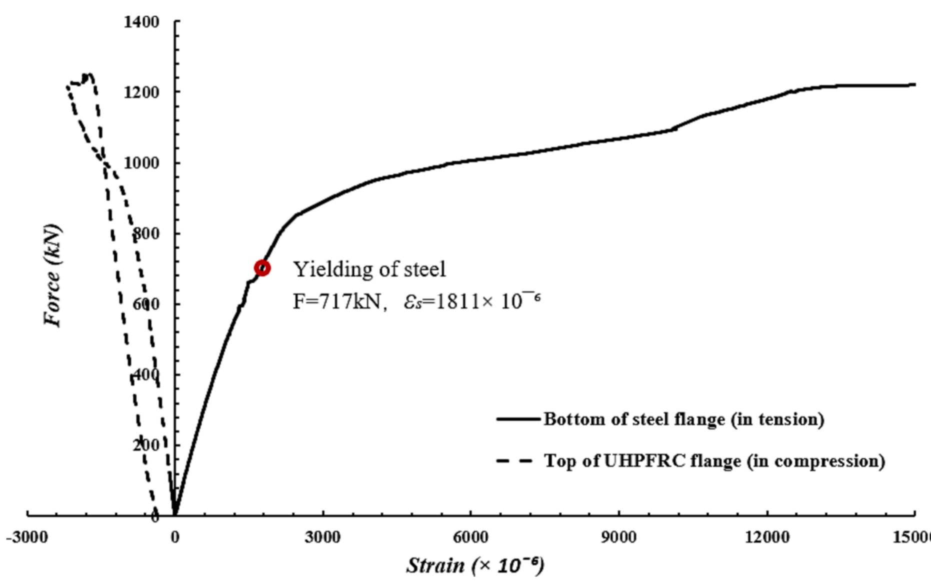

Fig. 11. Force vs. strain (F-ε) relationship in the middle section.

critically with slight increase of force. The peak force was reached when the second longitudinal steel rebar ruptured. In this domain, most of central deflection δ was developed while around 33 % of resistance was carried.

(5) Softening domain (DE).

In this domain, $w_{max} > 20.28$ mm, implying that UHPFRC provided little tensile contribution, while the steel component carried almost all the tensile force.

4.2. Shear behavior

4.2.1. Failure mode and shear-force vs. Deflection response

As illustrated in Fig. 15, B2 under 3PBT failed with one critical diagonal crack and several fine vertical and diagonal fictitious cracks (visible by the naked eyes), while no visible damage is observed on the steel component. The critical diagonal crack crossed the UHPFRC web at an angle of around 45°. It should be noted that the fibers between the crack still provided bridging effect without pull-out, and the crack end didn't penetrate into the UHPFRC flange.

Furthermore, the UHPFRC on one side of steel dowels was saw off to examine the interaction between UHPFRC and steel dowels, as shown in Fig. 15, in which the red dash lines stand for the original position of steel dowels. Obvious local crushing and cracks of UHPFRC in the recess between steel dowels behind the position of critical diagonal crack were noted. The steel dowels deformed accordingly and shifted longitudinally from their original positions, forced by the shift of UHPFRC due to the opening of critical diagonal crack. These phenomena imply the effective interlocking between UHPFRC and steel dowels, allowing the force transfer between dowels and thus avoiding element failure due to local failure. This can be attributed to the high mechanical properties of UHPFRC in both tension and compression, and the stirrups passing through the recess further improve this interlocking effect.

The shear-force vs. deflection (V-δ) response is presented in Fig. 16, in which the deflection was measured at the loading section excluding the deformation at the supports based on the measurement from LVDTs. A linear response is observed in the V-δ curve up to elastic limit (point

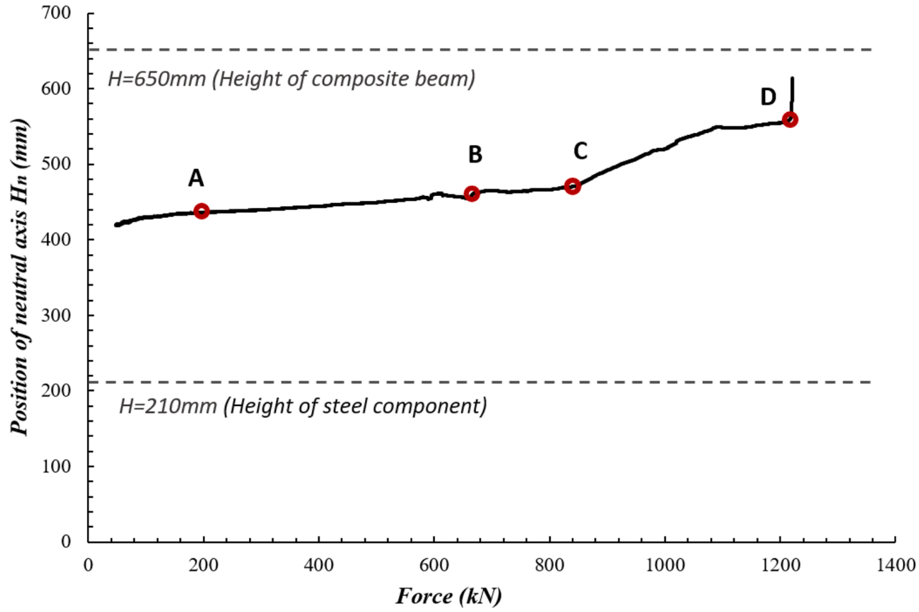

Fig. 12. Force vs. position of neutral axis (F-H_n) relationship in the middle section.

A), followed by a large non-linear part until the peak point (point D) and then a ductile softening domain.

4.2.2. Fracture behavior based on DIC analysis

Similarly, according to the fracture behavior on the critical shear crack region of UHPFRC web using DIC analysis (Fig. 17), the *V-δ* curve can be characterized into five different domains, as marked in Fig. 16. And the maximum opening of every single microcrack and fictitious crack given in Fig. 18. The main parameters for each characteristic point are summarized in Table 4. The determination of characteristic points is same as described in section 4.1.2.

(1) Elastic domain (OA).

Both UHPFRC and steel were in elastic phase, resulting in a linear V-δ curve up to elastic limit (point A, $V_A \approx 0.28 \cdot V_D$). At point A, several diagonal microcracks initiated on the middle part of the UHPFRC web.

(2) Quasi-elastic domain (AB).

More diagonal microcracks in parallel to the existing ones initiated on the UHPFRC web, and several secondary vertical (flexural) microcracks initiated on the lower part of UHPFRC web. At quasi-elastic limit (point B, $V_B \approx 0.70 \cdot V_D$), the diagonal microcracks distributed uniformly on the UHPFRC web with average spacing of around 22 mm, and the openings of these microcracks were mainly less than 0.1 mm. This domain developed around 42 % of shear resistance with slight loss of structural stiffness.

(3) Hardening domain (BC).

There was no new diagonal microcracks generated in this domain. As force increased, the existing microcracks propagated with generation of secondary microcracks, and some of them became fictitious cracks with opening larger than 0.15 mm.

(4) Yielding domain (CD).

At point C ($V_C \approx 0.90 \cdot V_D$), strain concentration mainly focused on one fictitious crack and its adjacent ones, as indicated in Fig. 17(c) by the red lines, implying the formation of critical diagonal crack. Afterward, the opening of critical shear crack increased rapidly, while the openings of other microcracks and fictitious cracks remained below 0.2 mm. At peak force (point D, F_D = 830.79 kN), the maximum opening of critical diagonal crack was 2.861 mm, which was far smaller than the case of UHPFRC web failure (the opening was larger than 10 mm as indicated in [23]). This can be attributed to the yielding of steel dowels as shown in Fig. 15, leading to failure of shear connectors and thus the drop of force.

(5) Softening domain (DE).

This domain still exhibited high ductility as shown in the V-δ curve. The opening of critical crack kept increasing fast, while the rest were closed partly with residual opening below 0.15 mm. It should be noted that the critical crack didn't propagate into top UHPFRC flange.

5. Discussion

Compared with the shear response of UHPFRC beam [36–38] and the existing steel-UHPFRC composite beam (Fig. 1-c) [24], the features of the proposed composite beam are indicated in this section.

As indicated in Fig. 15 and Fig. 17, the inclined angle of critical diagonal crack is around 45°, which is higher than that in UHPFRC beam. As reported by Ji et al. [37], the inclined angles were in the range of 29° to 40° for UHPFRC T-shaped beams with same shear slenderness ratio of 2 but different stirrup ratios and longitudinal reinforcement ratios. And a range of 23.4° to 35.6° was stated for UHPFRC I-shaped beams with different stirrup ratios and fiber volume contents by Mészöly et al. [36].

Furthermore, significant ductility was highlighted in the shear response of the proposed composite beam, where an obvious yielding domain was recognized (Fig. 16). This can be attributed to the existence of steel component, which restricted the propagation and widening of shear cracks. In the tensile zone of UHPFRC web, once the diagonal crack reached the level of steel component (inserted part), the widening of the crack was significantly restricted, thereby allowing consistent transfer of shear force. Simultaneously, strong dowel action was expected in this zone, and the hook-like end of the steel dowels reinforced the tensile strength of UHPFRC in vertical direction, preventing the horizontal cracks on UHPFRC web. Those resulted in continuous increase of shear force with generation and propagation of more diagonal microcracks and fictitious cracks in the rest of tensile zone, as illustrated in DIC strain contours (Fig. 17). On the other hand, in the compressive zone of UHPFRC web, the higher horizontal compressive stress induced by the larger bending moment and higher vertical compressive stress induced by higher imposed force due to the reinforcement effect from steel component were expected. Such great biaxial compressive state significantly enhanced the shear performance of UHPFRC web at compression zone, in which the propagation of diagonal cracks was delayed or even prevented at higher loading stages due to the consequent reduced principal tensile stress in the compression zone, especially as approaching to the loading point. Thus, it is reasonable that a large area adjacent to the loading point was free of (fictitious) cracks

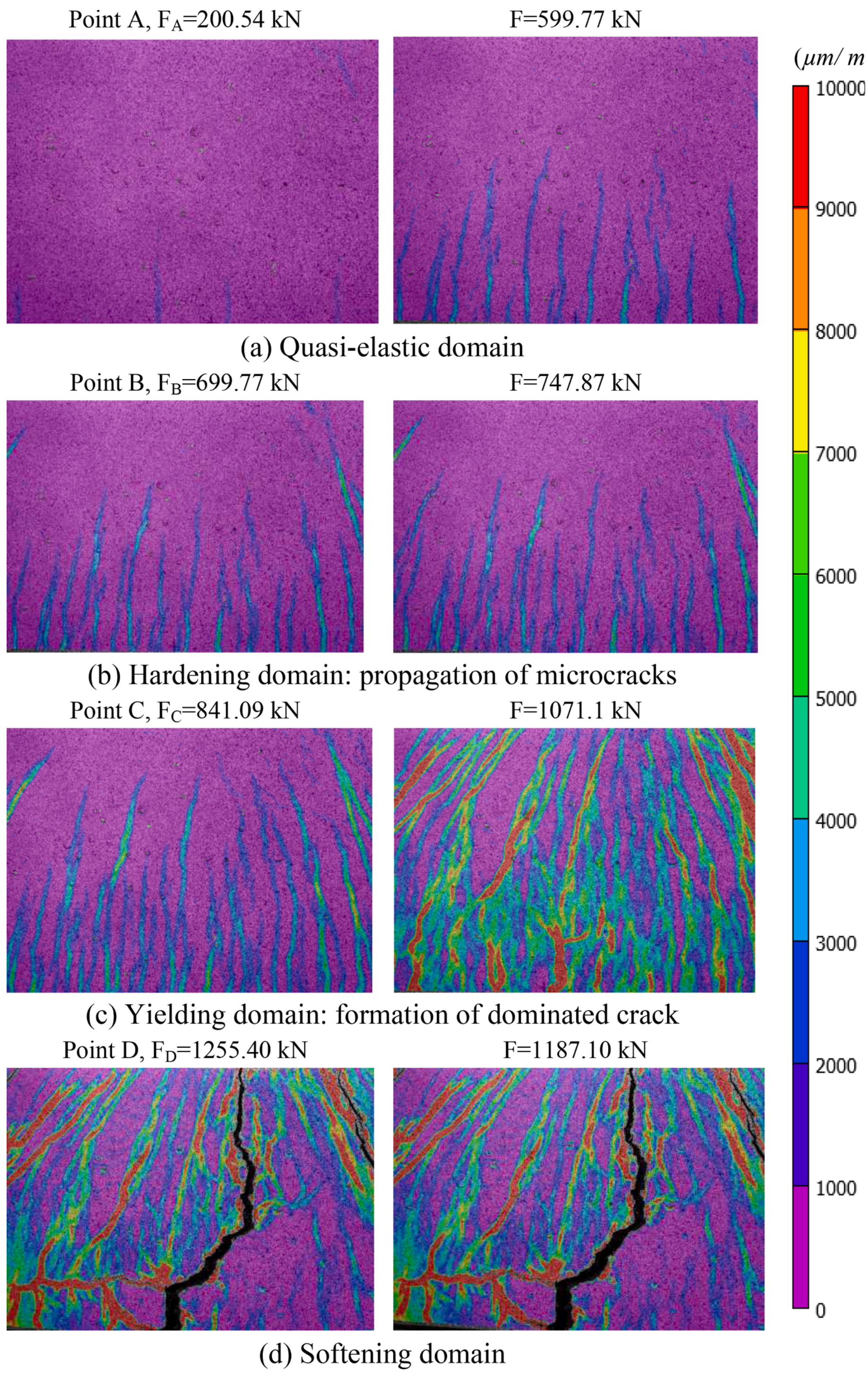

Fig. 13. Fracture response of B1 under 4PBT.

Table 3
Parameters for characteristic points of F-δ curve.

Point	F [kN]	δ [mm]	ε_{bottom} [10^{-6}]	w_{max} [mm]	H_n [mm]
A	192.34 ($\approx 0.15F_D$)	1.41	356	0.009	436
B	717.41 ($\approx 0.57F_D$)	6.74	1811	0.032	465
C	841.09 ($\approx 0.67F_D$)	9.17	2377	0.058	471
D	1255.40	93.93	>20000	20.286	>565

even up to failure, as shown in Fig. 15.

In addition, a relative ductile softening domain was observed in the composite beam. This can be explained by the failure mode of shear connection, where high ductility of steel dowel after yielding during degrading process still allowed redistribution of horizontal shear force towards unyielded ones. Such beneficial effect of shear force redistribution was also reported in [39].

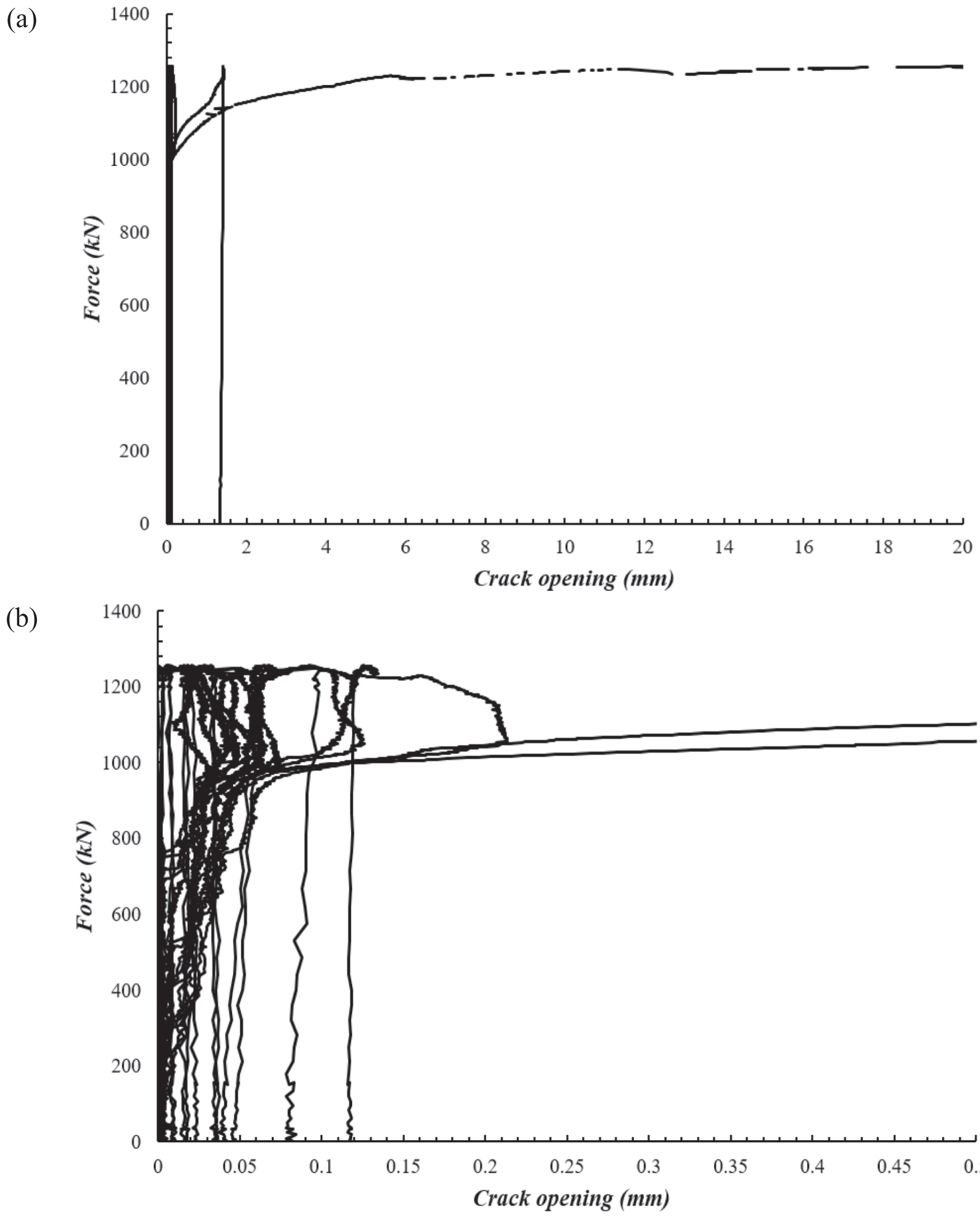

Fig. 14. Force vs. opening (F-w) response: (a) overview; (b) zoom in the opening up to 0.5 mm.

6. Design principles

6.1. Flexural resistance

The efficient interaction between steel and UHPFRC components are observed in section 4.1. At peak force, the advanced mechanical properties of UHPFRC and steel materials are fully utilized, as expected in Fig. 4. Thus, the sectional analysis method considering the tensile properties of UHPFRC, following the studies from Yoo et al.[20], is applied to predict the flexural resistance of proposed composite beam. As illustrated in Fig. 19, the cross section is subdivided into multiple layers, and the strain distribution is assumed to be linear along the height of cross section.

By assuming a value for ε_{bottom}, the strain ε_i in each layer is determined as Eq.(1), and the corresponding σ_i is calculated based on the stress–strain responses of UHPFRC and steel materials from rebars and rolled section. The specific position of neutral axis x_n can then be obtained giving that the resultants of the sectional forces in all the layers are in equilibrium, see Eq.(2). And the total moment M can be calculated using Eq.(3).

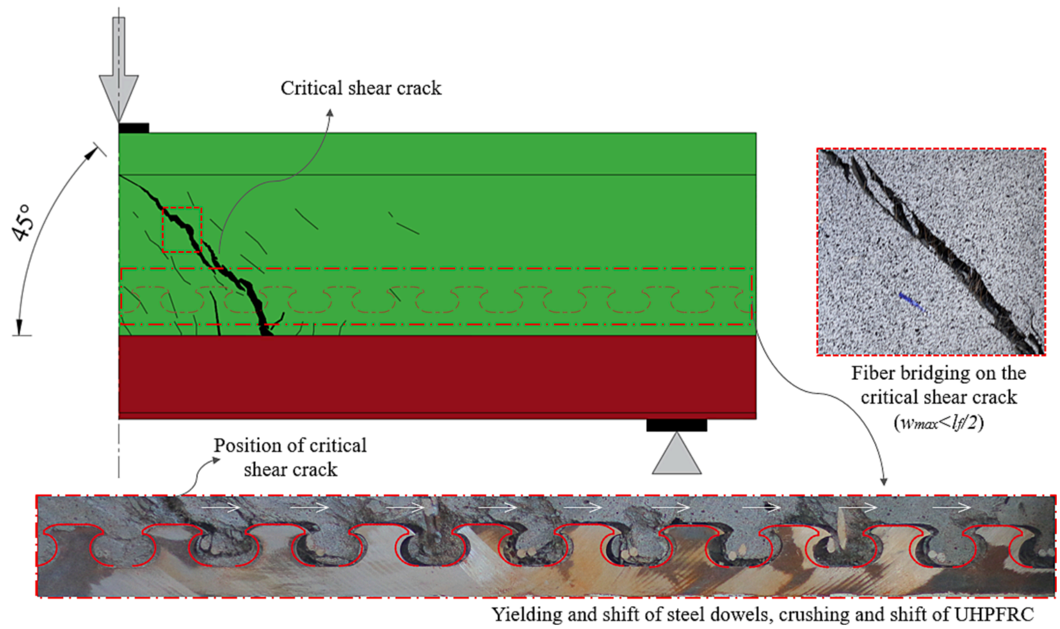

Fig. 15. Failure mode of B2 after testing.

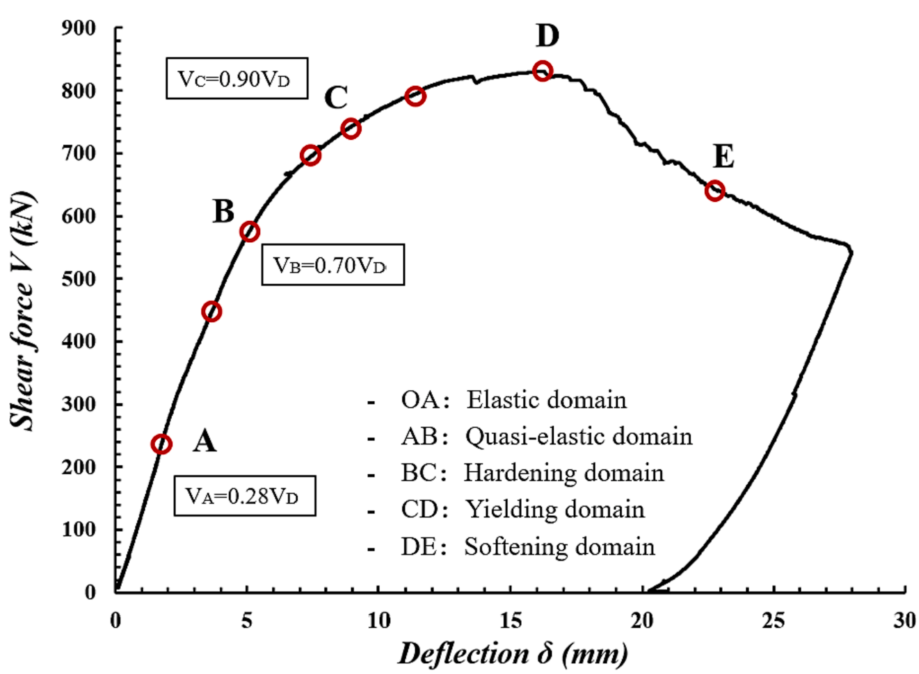

Fig. 16. Shear-force vs. deflection (V-δ) relationship from B2.

$$\varepsilon_i = \frac{x_i - x_n}{h - x_n} \bullet \varepsilon_{bottom} \tag{1}$$

$$F_{Uc} + F_{Ut} + F_{st} + F_{Ht} = 0$$

$$\int \sigma_i b_i dh + \int \sigma_s dA_s = 0 \tag{2}$$

$$M = \int \sigma_i b_i y_i dh + \int \sigma_s y_s dA_s \tag{3}$$

where b_i is the width of i^{th} layer; dh is the height of each layer; y_i is the distance between each neutral axis and i^{th} layer; σ_s and A_s are the stress and area of steel reinforcement, respectively.

The constitutive laws of UHPFRC and steel are simplified based on the material testing results in section 3.2. As shown in Fig. 20, for UHPFRC, a trilinear model in tension with fracture strain $\varepsilon_{Utr} = 0.01$, and a linear model up to compressive strength in compression, are adopted; for steel, an elastic–plastic model with fracture strain $\varepsilon_{sr} = 0.035$ is used.

Based MATLAB coding, the flexural resistance is determined to be 1231.32 kN when the maximum moment is reached using Eq.(3). This calculated value agrees well with the tested value (1255.40 kN). At this point, the strain at the bottom steel flange at critical section is calculated to be 0.035 and the whole section of steel component yield, and the strain at bottom of UHPFRC web reaches 0.022, suggesting the fracture of UHPFRC material without any strength. Those show agreement with

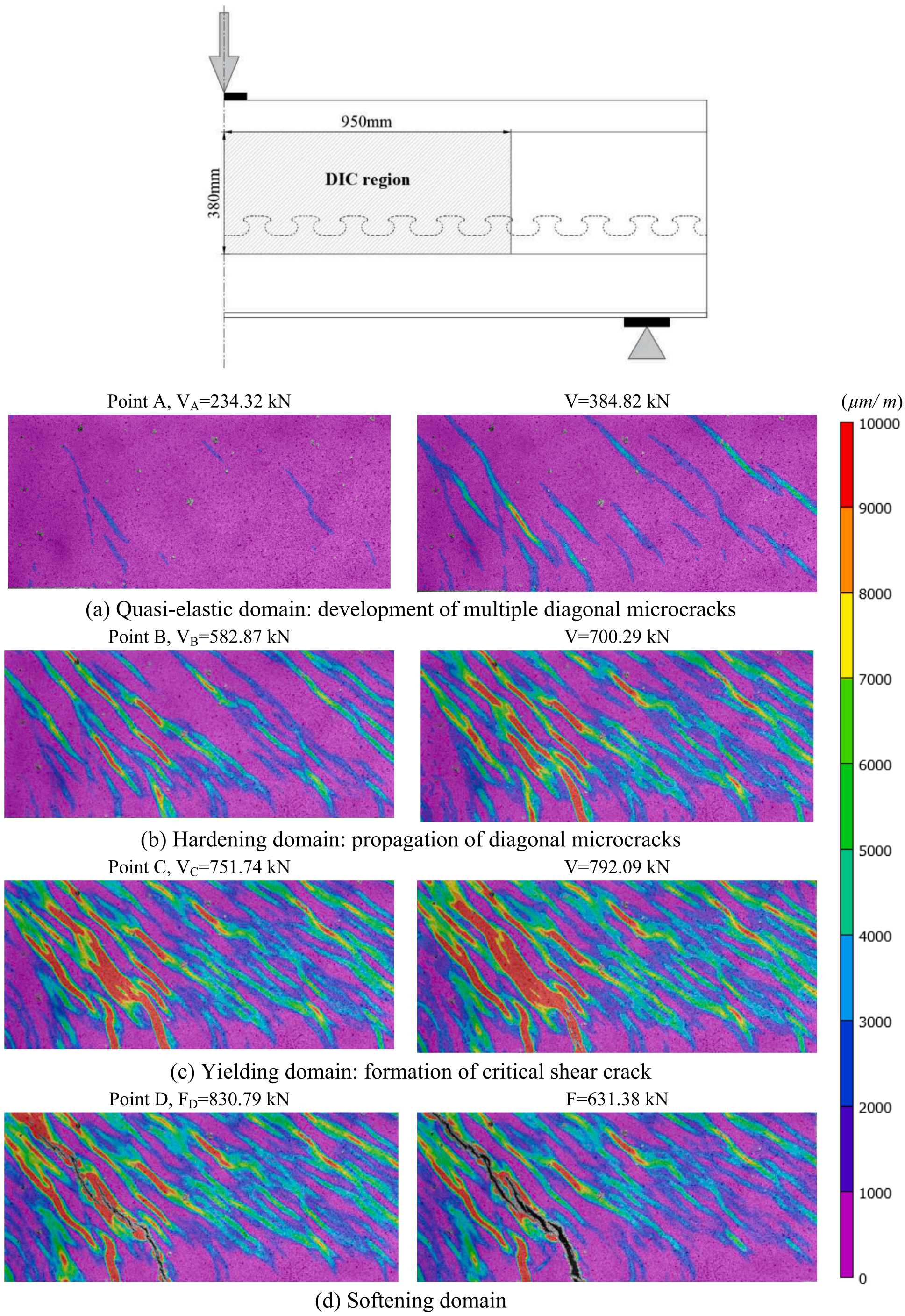

Fig. 17. Fracture process of B2 under 3PBT.

the experimental results in section 4.1.

6.2. Shear resistance

According to failure mode as described in 4.2, the shear resistance of present composite structure in proper design is governed by shear connection. Thus, following the idea on steel-NC composite beam from Lorenc et al. [29,40,41], the shear resistance can be calculated using Eq. (4):

$$V_R = v_L \bullet z \tag{4}$$

where v_L is the unit longitudinal shear resistance; z represents the lever arm between the resultants of compressive force and tensile force, $z \approx 0.9h$ is used based on previous sectional analysis.

As shown in Fig. 15, the yielding of steel dowels is observed when the peak force is reached. Thus, the longitudinal shear resistance of single composite dowel in slim UHPFRC element can be estimated following the study from Lechner [42], where the tensile contribution of UHPFRC was took into account:

$$P_{st} = 0.66 \bullet \left(\frac{f_{Utu} \bullet t_U}{f_y \bullet t_s}\right)^{0.4} \bullet f_y \bullet t_s \bullet e_x \tag{5}$$

where f_{Utu} is the tensile strength of UHPFRC; t_U is the thickness of UHPFRC element; e_x is the distance between two adjacent steel dowels;

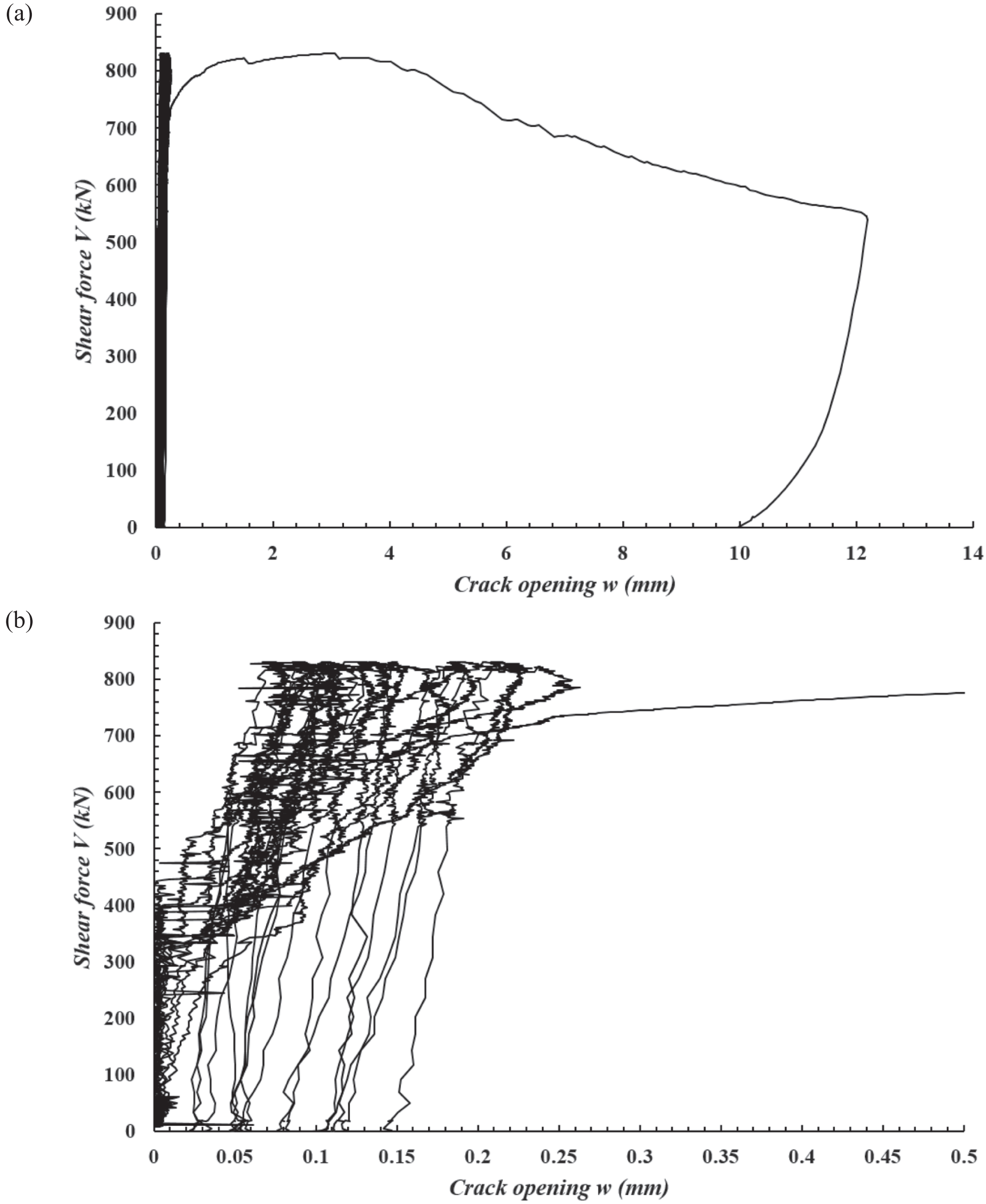

Fig. 18. Shear-force vs. opening (V-w) response: (a) overview; (b) zoom in the opening up to 0.5 mm.

Table 4
Parameters for characteristic points of V-δ curve.

Point	***V*** *[kN]*	***δ*** *[mm]*	ε_{bottom} [10–6]	w_{max} *[mm]*
A	234.32 ($\approx 0.28V_D$)	1.73	464	0.030
B	582.87 ($\approx 0.70F_D$)	5.19	1089	0.167
C	751.74 ($\approx 0.90F_D$)	9.32	2778	0.615
D	830.79	16.20	5651	2.861

t_s is the thickness of steel dowel; f_y is the yielding strength of steel.

Accordingly, the calculated shear resistance is 806.04 kN, in agreement with the tested value (830.79kN).

7. Conclusions

The present study proposes a new steel-UHPFRC composite beam structure, where the unique use of ① UHPFRC in both tension and compression and ② half rolled section with in-built steel dowels in combination with UHPFRC dowels (forming composite dowels as shear connectors) is highlighted. An experimental program is then developed

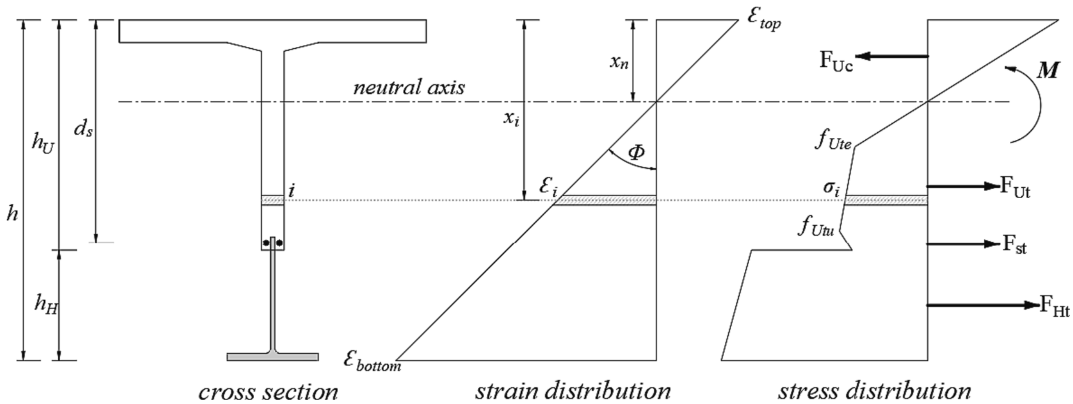

Fig. 19. Schematic multi-layered section, strain and stress distribution of composite beam.

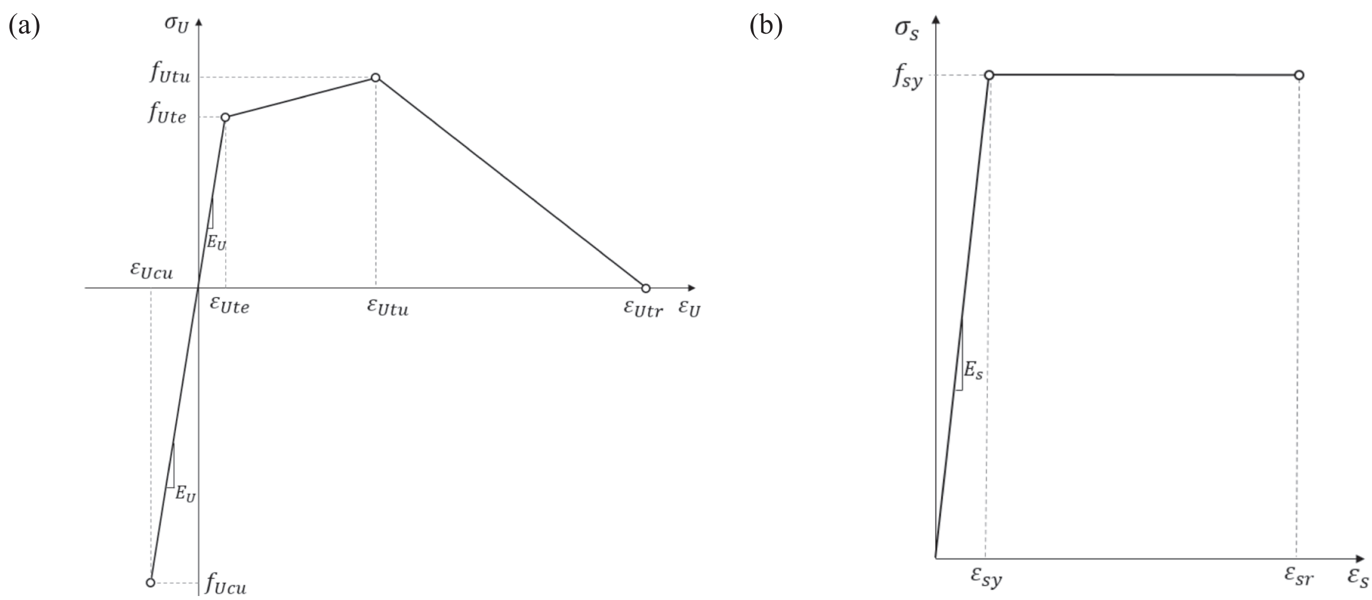

Fig. 20. Simplified material constitutive laws of (a) UHPFC; and (b) steel.

to investigate the structural response of the composite beam in both bending and shear, and the design principles for flexural and shear resistance were introduced and validated based on experimental results.

The main conclusions of this investigation are given below:

(1) The effective interlocking between UHPFRC and steel dowels allows efficient interaction between UHPFRC and steel components, and thus full utilization of both UHPFRC and steel materials under positive moment. At peak force, the whole section of steel component yielded, the dominant crack of UHPFRC had opening > 20 mm and the top UHPFRC flange crushed.
(2) The flexural response of composite beam can be characterized into 5 distinguished domains. Especially, the quasi-elastic domain is introduced, given that around 42 % of resistance was developed with slight increase of deflection in this domain, resulting in almost linear F-δ response and comparable structural stiffness with the original one. At the elastic limit (point B, $F_B \approx 0.57 \cdot F_D$), the bottom steel flange started to yield, and most of the UHPFRC part in tension were in hardening phase (w_{max} = 0.032 mm) with average microcrack spacing below 20 mm.
(3) The updated sectional analysis method considering the tensile properties of UHPFRC can accurately predict the flexural resistance of the composite beam.
(4) The shear fracture behavior of the composite beam is governed by the combined degradation of the UHPFRC web and composite dowels, while the steel dowel yielding leads to the drop of shear force. And the high ductility of composite dowels still allows strong redistribution of horizontal shear force, resulting in relatively ductile fracture process in softening domain.
(5) The shear response of composite beam can also be characterized in to 5 distinguished domains. At the elastic limit (point B, $V_B \approx 0.70 \cdot V_D$), uniform distribution of diagonal microcracks with average spacing below 22 mm is observed on UHPFRC web. Furthermore, an obvious yielding domain is highlighted. These can be attributed to the existence of steel component as external reinforcement, thus restricting the propagation and widening of shear cracks due to enhancement in chord effect and compression zone of UHPFRC web.
(6) The shear resistance of composite beam can be predicted accurately based on a special approach to the lever arm of internal forces and horizontal shear resistance of composite dowel considering the tensile contribution of UHPFRC.

CRediT authorship contribution statement

Yaobei He: Validation. **Xiujiang Shen:** Conceptualization, Methodology, Resources, Writing – original draft, Writing – review & editing, Data curation, Funding acquisition. **Guang Chen:** Validation. **Xudong Shao:** Validation.

Declaration of Competing Interest

The authors declare that they have no known competing financial interests or personal relationships that could have appeared to influence the work reported in this paper.

Data availability

No data was used for the research described in the article.

Acknowledgement

The financial supports from the National Natural Science Foundation of China (No. 52108138), the Youth Science and Technology Innovation Talent Project of Hunan Province (2020RC3081) and the Hunan Traffic Science and Technology Project (No. 202245) are greatly appreciated.

References

[1] Scrivener KL, John VM, Gartner EM. Eco-efficient cements: Potential economically viable solutions for a low-CO2 cement-based materials industry. Cem Concr Res 2018;114:2–26. https://doi.org/10.1016/j.cemconres.2018.03.015.

[2] Davis SJ, Lewis NS, Shaner M, Aggarwal S, Arent D, Azevedo IL, et al. Net-zero emissions energy systems. Science 2018;360:eaas9793. https://doi.org/10.1126/science.aas9793.

[3] Sustainable Development & Energy | ASCE n.d. https://www.asce.org/advocacy/energy/ .

[4] Dean B, Dulac J, Petrichenko K, Graham P. Towards zero-emission efficient and resilient buildings. Global Status Report 2016.

[5] Bien J, Elfgren L, Olofsson J. Sustainable bridges : assessment for future traffic demands and longer lives. Dolnoslaskie Wydawnictwo Edukacyjne 2007.

[6] Richard P, Cheyrezy M. Composition of reactive powder concretes. Cem Concr Res 1995;25:1501–11.

[7] Yu R, Spiesz P, Brouwers HJH. Mix design and properties assessment of Ultra-High Performance Fibre Reinforced Concrete (UHPFRC). Cem Concr Res 2014;56:29–39. https://doi.org/10.1016/j.cemconres.2013.11.002.

[8] Shen X, Brühwiler E. Influence of local fiber distribution on tensile behavior of strain hardening UHPFRC using NDT and DIC. Cement and Concrete Research 2020;132:106042. https://doi.org/10.1016/j.cemconres.2020.106042.

[9] Shen X, Brühwiler E, Peng W. Biaxial flexural response of Strain-Hardening UHPFRC circular slab elements. Constr Build Mater 2020;255:119344. https://doi.org/10.1016/j.conbuildmat.2020.119344.

[10] Makita T, Brühwiler E. Tensile fatigue behaviour of ultra-high performance fibre reinforced concrete (UHPFRC). Mater Struct 2014;47:475–91. https://doi.org/10.1617/s11527-013-0073-x.

[11] Makita T, Brühwiler E. Tensile fatigue behaviour of Ultra-High Performance Fibre Reinforced Concrete combined with steel rebars (R-UHPFRC). Int J Fatigue 2014;59:145–52.

[12] Parant E, Rossi P, Boulay C. Fatigue behavior of a multi-scale cement composite. Cem Concr Res 2007;37:264–9. https://doi.org/10.1016/j.cemconres.2006.04.006.

[13] Chanvillard G, Pimienta P, Pineaud A, Rivillon P. Fatigue flexural behavior of pre-cracked specimens of special UHPFRC. Special Publication 2005;228:1253–68.

[14] Farhat FA, Nicolaides D, Kanellopoulos A, Karihaloo BL. High performance fibre-reinforced cementitious composite (CARDIFRC)–Performance and application to retrofitting. Eng Fract Mech 2007;74:151–67.

[15] Shen X, Brühwiler E. Biaxial flexural fatigue behavior of strain-hardening UHPFRC thin slab elements. Int J Fatigue 2020;138:105727. https://doi.org/10.1016/j.ijfatigue.2020.105727.

[16] Brühwiler E. UHPFRC technology to enhance the performance of existing concrete bridges. Struct Infrastruct Eng 2020;16:94–105. https://doi.org/10.1080/15732479.2019.1605395.

[17] Graybeal B, Brühwiler E, Kim B-S, Toutlemonde F, Voo YL, Zaghi A. International Perspective on UHPC in Bridge Engineering. J Bridg Eng 2020;25:04020094. https://doi.org/10.1061/(ASCE)BE.1943-5592.0001630.

[18] Benedetty CA, dos Santos VB, Krahl PA, Rossi A, de Silva F, A, Cardoso DCT, et al. Flexural and shear behavior of steel-UHPC composite beams: a review. Eng Struct 2023;293:116649. https://doi.org/10.1016/j.engstruct.2023.116649.

[19] Deng S, Shao X, Zhao X, Wang Y, Wang Y. Precast steel—UHPC lightweight composite bridge for accelerated bridge construction. Front Struct Civ Eng 2021. https://doi.org/10.1007/s11709-021-0702-3.

[20] Yoo S-W, Choo JF. Evaluation of the flexural behavior of composite beam with inverted-T steel girder and steel fiber reinforced ultra high performance concrete slab. Eng Struct 2016;118:1–15. https://doi.org/10.1016/j.engstruct.2016.03.052.

[21] Wang K, Zhao C, Wu B, Deng K, Cui B. Fully-scale test and analysis of fully dry-connected prefabricated steel-UHPC composite beam under hogging moments. Eng Struct 2019;197:109380. https://doi.org/10.1016/j.engstruct.2019.109380.

[22] Zhu J, Guo X, Kang J, Duan M, Wang Y. Numerical and theoretical research on flexural behavior of steel-UHPC composite beam with waffle-slab system. J Constr Steel Res 2020;171:106141. https://doi.org/10.1016/j.jcsr.2020.106141.

[23] Shao X, Zhao X, Liu Q, Deng S, Wang Y. Design and experimental study of hot rolled shape steel-ultrahigh performance concrete composite beam. Eng Struct 2021::113612. https://doi.org/10.1016/j.engstruct.2021.113612.

[24] Zhao X, Shao X, Cao J, Shao Z, Ying-Li R. Experimental studies on shear behavior of steel-UHPC composite beam with hot rolled shape steel. Eng Struct 2023;274:115160. https://doi.org/10.1016/j.engstruct.2022.115160.

[25] Lorenc W. Composite dowels: the way to the new forms of steel-concrete composite structures. Poland: Wrocław; 2020.

[26] Feldmann M, Kopp M, Pak D. Composite dowels as shear connectors for composite beams – background to the German technical approval. Steel Construction 2016;9:80–8. https://doi.org/10.1002/stco.201610020.

[27] Kopp M, Wolters K, Claßen M, Hegger J, Gündel M, Gallwoszus J, et al. Composite dowels as shear connectors for composite beams – Background to the design concept for static loading. J Constr Steel Res 2018;147:488–503. https://doi.org/10.1016/j.jcsr.2018.04.013.

[28] Petzek E, Schmitt V, Meteş E, Ispăşoiu G, Ţurcan A. Romanian projects and integral bridge solutions based on composite dowels. Steel Construction 2016;9:161–9. https://doi.org/10.1002/stco.201610022.

[29] Lorenc W, Kurz W, Seidl G. Hybrid steel–concrete sections for bridges: Definition and basis for design. Eng Struct 2022;270:114902. https://doi.org/10.1016/j.engstruct.2022.114902.

[30] Harsányi P, Randl N, Tue NV. DIC-based failure analysis of high-strength continuous steel shear dowels for composite UHPFRC steel construction. Eng Struct 2021;247:113093. https://doi.org/10.1016/j.engstruct.2021.113093.

[31] Lechner T, Gehrlein S. Structural behaviour of composite dowels in thin UHPC elements. Steel Construction 2016;9(2):132–7.

[32] Deutsches Institut für Bautechnik. Allgemeine Bauaufsichtliche Zulassung Z-26.4-56: Verbunddübelleisten. 2013.

[33] Heinemeyer S. Zum Trag-und Verformungsverhalten von Verbundträgern aus ultrahochfestem Beton mit Verbundleisten. Aachen: Eigenverl; 2011.

[34] Pam HJ, Kwan AKH, Islam MS. Flexural strength and ductility of reinforced normal- and high-strength concrete beams. Proceedings of the Institution of Civil Engineers - Structures and Buildings 2001;146:381–9. https://doi.org/10.1680/stbu.2001.146.4.381 .

[35] Zhan J, Denarié E, Brühwiler E. Elastic limit tensile stress of UHPFRC: Method of determination and effect of fiber orientation. Cem Concr Compos 2023::105122. https://doi.org/10.1016/j.cemconcomp.2023.105122.

[36] Mészöly T, Randl N. Shear behavior of fiber-reinforced ultra-high performance concrete beams. Eng Struct 2018;168:119–27. https://doi.org/10.1016/j.engstruct.2018.04.075.

[37] Ji W, Li W, An M, Zhu L. Shear Capacity of T-Section Girders Made of Reactive Powder Concrete. J Bridg Eng 2018;23:04018041. https://doi.org/10.1061/(ASCE)BE.1943-5592.0001253.

[38] Schramm N, Fischer O. Precast bridge construction with UHPFRC—Shear tests and railway bridge pilot application. Civil Engineering Design 2019;1:41–53. https://doi.org/10.1002/cend.201800005.

[39] Christou G, Hegger J, Classen M. Multi-span composite girders with composite dowels – Experimental investigations and design approach to account for the beneficial effect of shear force redistribution along the composite interface. Eng Struct 2023;285:115944. https://doi.org/10.1016/j.engstruct.2023.115944.

[40] Johnson RP. Vertical shear in hybrid composite cross-sections of beams. Poland: Warsaw; 2021.

[41] Seidl G, Schmitt V, Lorenc W. Brücken mit Verbunddübelleisten - Entwurf, Bemessung und Ausführungsbeispiele, Dresdner, Germany: June 7-8, 2022; n.d.

[42] Lechner T. Zur Anwendung von Verbunddübelleisten in schlanken Verbundträgern aus ultrahochfestem Beton. Technische Universität München; 2018.